A Modified Real-Valued Feed-Forward Neural Network Low-Pass Equivalent Behavioral Model for RF Power Amplifiers

Luiza B. Chipansky Freire, Caroline de França, and Eduardo G. de Lima*

Abstract—This work addresses the low-pass equivalent behavioral modeling of radio frequency (RF) power amplifiers (PAs) for modern wireless communication systems. Similar to a previous approach, here the PA behavioral modeling is based on two independent real-valued feed-forward artificial neural networks (ANNs). A careful analysis is first presented to show that the nonlinear training algorithm for the previous ANN-based approach can be easily trapped into local minima, especially for the ANN that estimates the polar angle component of a complex-valued signal. Then, a modified ANN-based model is proposed to eliminate the local minimum problem, in this way significantly improving the modeling accuracy. Indeed, in the proposed model the two real-valued ANNs are responsible for estimating the in-phase and quadrature components of a complex-valued base-band signal. When applied to the behavioral modeling of a GaN HEMT class AB PA, the proposed ANN-based model reduces normalized mean-square error (NMSE) by up to 2.2 dB, in comparison with the previous ANN-based model having an equal number of network parameters.

1. INTRODUCTION

Linearity is an obligatory requirement in modern cellular systems [1]. Indeed, the providers of cellular services can only comply with the agreed high data rates and acceptable levels of quality if rigorous linearity specifications are completely satisfied. The frequency spectrum is shared among a large set of completely different applications, and therefore, the bandwidth allocated to cellular systems is very narrow. In this context, a fundamental concern is the adoption of a strategy to allow for an efficient use of the bandwidth, in the sense of achieving higher data rates in the fixed available bandwidth. Actually, a significant augment in the rate of data transmission is possible if, besides the phase, the amplitude of a radio frequency (RF) carrier signal is also allowed to be changed as a function of the information signal [2]. However, an amplitude modulated RF carrier demands for linearity. While the information signal preserves its bandwidth when applied to a linear operator, the same is not true when it is subject to a nonlinear operator. This is because nonlinear operators can give rise to non-negligible contributions at frequencies not excited by the applied input information signal. As a consequence, the bandwidth of an amplitude modulated RF carrier signal can be widened after the signal is processed thought any nonlinearity. The bandwidth widening dramatically deteriorates the system quality because neighbor users will interfere with each other.

The traditional design of highly linear wireless transmitters critically impacts the overall power efficiency of the system [3]. In particular, power amplifiers (PAs) based on semiconductor transistors polarized in class A, AB or B are linear only when driven at lower power levels. On the other hand, to optimize its power efficiency, the PA must operate near its maximum power, at strong gain compression, producing non-negligible nonlinear distortions. Therefore, to comply with the linearity requirements,

the PA efficiency is very poor. This has serious consequences, especially because the PA is the circuit that consumes the largest amount of energy in the wireless communication system. Thus, a lot of effort is been pushed toward high efficiency, especially for extending the battery autonomy in handsets and relaxing the demand for heat dissipation in base-stations [4, 5].

To obtain high efficiency at the same time keeping the linearity within mandatory thresholds, a common approach is to include, in the transmitter chain, a linearization scheme known in literature as digital base-band predistortion (DPD) [6]. An accurate model for the PA, which relates complex-valued envelope signals and is capable of predicting nonlinear dynamic behaviors observed in PAs with reduced computational cost, is essential to designing a DPD that works properly [7–13]. A real-valued feed-forward artificial neural network (ANN), when excited by the same complex-valued envelope signal applied to the PA input and after proper supervised training, can mimic the PA dynamic nonlinear behaviors and, in this way, generate a complex-valued envelope signal very close to the measured PA output signal [10].

In literature, great efforts have been spent to obtain more accurate predictions for the PA complex-valued output envelope based on real-valued ANNs with fewer network parameters (weights and biases) [10–13]. For such purpose, the strategy followed in [10–12] was to change the real-valued signals applied as ANN inputs. In fact, for applying real-valued ANNs to the low-pass equivalent PA behavioral modeling, complex-valued signals must be first transformed into real-valued signals to only then be applied to the ANN inputs. In particular, a decomposition based on amplitude and phase difference components [12] was reported to produce a better compromise than the traditional Cartesian [10] and polar [11] decompositions. Additionally, [13] reported the advantages of using two independent ANNs (of single output) with respect to the use of a unique ANN having two outputs. Moreover, for applying real-valued ANNs to the low-pass equivalent PA behavioral modeling, real-valued signals at the ANN outputs must be somehow combined to obtain a complex-valued estimation. However, the impacts on modeling accuracy of constructing one complex-valued signal from two real-valued signals estimated by the ANNs were not investigated in [10–13]. The novelties of this work are the following. First, it identifies the main impacts that the choice for the mapping from two real-valued to one complex-valued signals can have on modeling accuracy. Second, it is observed that the choices for such mapping made by previous approaches can critically affect the modeling accuracy because the ANN training algorithm can be easily trapped into local minima. Third, it proposes an alternative mapping that has the advantage of turning the ANN training algorithm less susceptible to the local minimum problem, and therefore, can produce a better trade-off between modeling accuracy and computational complexity. In other words, here a novel strategy is adopted to further improve the modeling accuracy of feed-forward ANNs. Specifically, the main contribution of this work is to propose a behavioral model that differs from the previous approach of [13] by the real-valued signals that must be estimated by the ANNs. In fact, in the proposed model, the ANNs are trained to estimate the real and imaginary parts of a complex-valued base-band signal.

This work is organized as follows. Section 2 describes low-pass equivalent PA behavioral modeling, and Section 3 briefly reviews feed-forward ANNs. Section 4 introduces the modified ANN-based model, and its advantages over previous approaches are carefully investigated, with particular attention to the local minima problem in the ANN training algorithm. Experimental data reported in Section 5 show that a better trade-off between model fidelity and number of network parameters is achieved by the novel approach. Conclusions are given in Section 6.

2. LOW-PASS EQUIVALENT POWER AMPLIFIER BEHAVIORAL MODELING

Let a PA be excited by the band-pass signal:

$$x = \Re\left[\tilde{x} \exp\left(j\omega_C t\right)\right] = a_x \cos\left(\omega_C t + \theta_x\right), \tag{1}$$

where ω_C is the carrier frequency on the order of GHz, $\tilde{x}$ the complex-valued envelope signal having a bandwidth of several MHz, a_x the amplitude component of $\tilde{x}$, and θ_x the polar angle component of $\tilde{x}$. When a PA is operated at strong compression gain and near saturation, nonlinear intermodulation (at the vicinity of ω_C) and harmonic distortions are generated. The PA output matching network reduces the contributions at harmonic frequencies of ω_C to negligible levels, and thus, the measured signal at

the PA output can be accurately written as:

$$y = \Re\left[\tilde{y}\exp\left(j\omega_C t\right)\right] = a_y\cos\left(\omega_C t + \theta_y\right), \tag{2}$$

where $\tilde{y}$ is the complex-valued output envelope signal, a_y the amplitude component of $\tilde{y}$, and θ_y the polar angle component of $\tilde{y}$. The nonlinear intermodulation distortions introduced by the PA are not attenuated by the output matching network and can be clearly observed in measurements performed at the PA output. Therefore, an accurate PA behavioral model has to map the output signal as a nonlinear function of the input signal. Additionally, non-ideal frequency responses of the bias circuit and the input and output matching networks give rise to dynamic effects that have a significant impact on the measured signal at the PA output [7]. In order to take into account dynamic effects, a non-recursive discrete-time model must calculate the PA output signal at the instantaneous time sample as a function of the PA input signal at instantaneous and previous time samples. Two different PA behavioral models are available, differing from each other by the kind of input and output signals handled by them [7]. In a band-pass model, the band-pass output at the instantaneous time sample (n) is given by:

$$y(n) = f_{BP}\left[x(n), x(n-1), \ldots, x\left(n - M_{BP}\right)\right], \tag{3}$$

where f_{BP} indicates an arbitrary band-pass nonlinear operator, and M_{BP} is the number of previous samples required by the band-pass model. In a low-pass equivalent model, the complex-valued envelope output at the instantaneous time sample (n) is computed using:

$$\tilde{y}(n) = f_{LPE}\left[\tilde{x}(n), \tilde{x}(n-1), \ldots, \tilde{x}(n - M_{LPE})\right], \tag{4}$$

where f_{LPE} indicates an arbitrary low-pass equivalent nonlinear operator and M_{LPE} the number of previous samples required by the low-pass equivalent model. Observe that a band-pass model describes the relationship between the band-pass signals x and y, while in a low-pass equivalent model only the relation between $\tilde{x}$ and $\tilde{y}$ is obtained.

To improve the modeling accuracy, the instantaneous output sample must be formulated as a function of the input applied at instantaneous and previous samples up to the longest memory effect intended to be represented by the model. Independent of the particular choice between a band-pass and a low-pass equivalent model, the memory length must be set to a same value on the order of the reciprocal of the envelope bandwidth (on the MHz range) to take into account long-term memory effects attributed to non ideal frequency response of the bias circuit [7]. Nevertheless, the time interval between two consecutive samples changes drastically based on the choice between a band-pass and a low-pass equivalent model. Indeed, the maximum allowed sampling interval must comply with the Nyquist criterion [14]. While the maximum frequency that must be handled by a band-pass model is equal to several harmonics of ω_C (on the GHz range), the low-pass equivalent model deals with signals having much lower bandwidths (on the order of the envelope bandwidth). Hence, to provide similar model fidelity, the band-pass model requires a much higher number of computations than the low-pass equivalent one. In fact, the huge amount of additional computations performed by a band-pass model only provides a clear picture of the frequency spectrum, as explained in the following. If a continuous-time signal is uniformly sampled in time, its original frequency-domain content is replicated in frequency at integer multiples of the sampling frequency. In a band-pass model, the replicas are separated to each other by a large distance, on the order of several harmonics of ω_C, and therefore, one can easily distinguish between in-band and out-of-band contributions by a simple visual inspection of the frequency spectrum. Conversely, in a low-pass equivalent model, due to the reduced sampling frequency, the fundamental and harmonic bands are superimposed to each other in the frequency-domain, e.g., all the bands are centered around the zero frequency. As a consequence, a frequency spectrum analysis over a low-pass equivalent model is no longer enough to distinguish between in-band (at the vicinity of ω_C) and out-of-band (at harmonic frequencies of ω_C) contributions. Once out-of-band contributions are not observed at the PA output, the use of a low-pass equivalent model that produces out-of-band contributions will perform useless computations that, however, can be responsible for a considerable fraction of the computational cost of a model. A computationally efficient low-pass equivalent model that performs only useful calculations must, therefore, generate only in-band contributions, which is mathematically equivalent to state that the integer number one that multiplies the carrier frequency (ω_C) is forbidden to be changed [12, 15].

3. REAL-VALUED FEED-FORWARD NEURAL NETWORKS

Figures 1(a) and 1(b) show the block diagrams of the two largely employed real-valued feed-forward artificial neural networks: the three-layer perceptron (TLP) and the radial-basis function (RBF) [16]. Observe that in Figures 1(a) and 1(b), the networks have E inputs, S outputs and R neurons in the hidden layer.
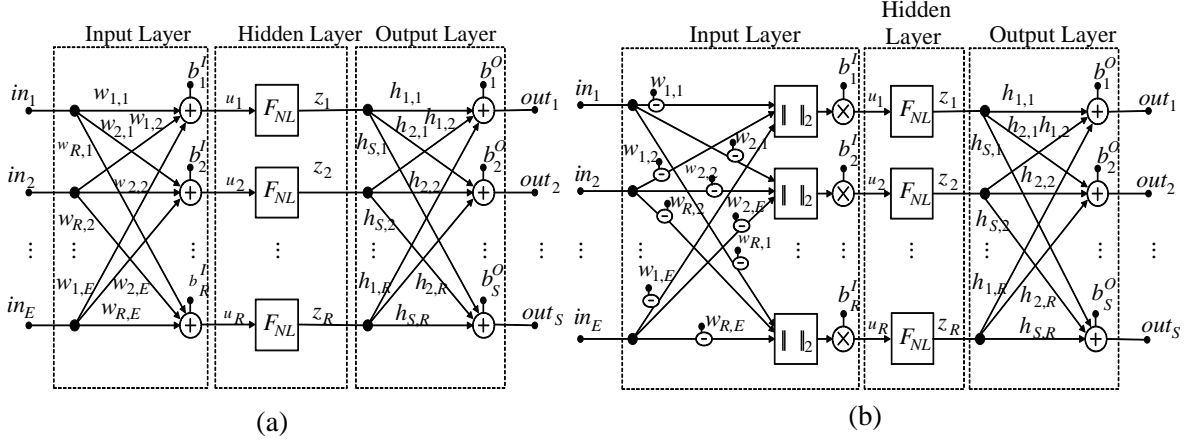
Figure 1. Block diagram of neural networks: (a) three-layer perceptron and (b) radial basis function.

A major difference between a TLP and an RBF is observed in the input layer, whereas the TLP input signals are manipulated by

$$u_r = b_r^I + \sum_{e=1}^{E} w_{r,e} in_e, \qquad (5)$$

the RBF input signals are modified according to

$$u_r = b_r^I \sqrt{\sum_{e=1}^{E} (in_e - w_{r,e})^2}. \qquad (6)$$

In (5) and (6), $w_{r,e}$ (with $r = 1, 2, \ldots, R$ and $e = 1, 2, \ldots, E$) are the input weights, and b_r^I (with $r = 1, 2, \ldots, R$) are the input biases. In the hidden layer, each signal u_r (with $r = 1, 2, \ldots, R$) is applied to a nonlinear operator F_{NL}. Indeed, the hyperbolic tangent sigmoid function

$$z_r = F_{NL}(u_r) = \frac{2}{1 + \exp(-2u_r)} - 1, \qquad (7)$$

is the common choice for TLP-based networks, while the Gaussian function

$$z_r = F_{NL}(u_r) = \exp\left(-u_r^2\right), \qquad (8)$$

is more commonly found in RBF-based networks.

The output layer is exactly the same for both TLP and RBF. For instance, the S network outputs $(out_1, out_2, \ldots, out_S)$ are given by:

$$out_s = b_s^O + \sum_{r=1}^{R} h_{s,r} z_r, \qquad (9)$$

where $h_{s,r}$ (with $r = 1, 2, \ldots, R$ and $s = 1, 2, \ldots, S$) are the output weights, and b_s^O (with $s = 1, 2, \ldots, S$) are the output biases.

To obtain the network parameters $w_{r,e}$, b_r^I, $h_{s,r}$ and b_s^O, a supervised training algorithm must be used in order to minimize the mean square error between desired and estimated outputs. Back-propagation [16] and orthogonal least-squares [17] are the standard algorithms for TLP and RBF trainings, respectively.

4. THEORETICAL DEVELOPMENT

Low-pass equivalent PA behavioral models discussed in Section 2 relate complex-valued envelope signals. Feed-forward ANNs addressed in Section 3 can only process real-valued signals. Therefore, in order to apply real-valued ANNs to the low-pass equivalent PA behavioral modeling, complex-valued signals must be first transformed into real-valued signals to only then be applied to the ANN inputs. Moreover, real-valued signals at the ANN outputs must be somehow combined to obtain a complex-valued estimation for the output envelope.

In [12], it was observed that the conversion from complex-valued into real-valued signals has a significant impact on the accuracy and computational complexity of a low-pass equivalent model. Traditionally, a complex-valued input envelope $\tilde{x}$ can be decomposed into amplitude (a_x) and polar angle (θ_x) components, according to

$$\tilde{x} = a_x \exp\left(j\theta_x\right), \tag{10}$$

or, equivalently, into real ($\Re_x$) and imaginary ($\Im_x$) parts,

$$\tilde{x} = \Re_x + j\Im_x, \tag{11}$$

where $\Re_x = a_x \cos(\theta_x)$ and $\Im_x = a_x \sin(\theta_x)$. If the rectangular (10) or polar (11) decompositions are employed to obtain the ANN real-valued inputs, out-of-band contributions are generated by the low-pass equivalent model. However, according to Section 2, a computationally efficient low-pass equivalent behavioral model must generate only in-band contributions. Once the polar angle component θ_x is related to the carrier frequency ω_C by ($\omega_C t + \theta_x$), in order to preserve the $1\omega_C t$, the θ_x cannot be directly applied as an ANN input. In fact, if θ_x is used as an ANN input, nonlinear activation functions in the hidden layer of an ANN can change the value of the integer number that multiplies ω_C. Furthermore, the real ($\Re_x$) and imaginary ($\Im_x$) components cannot be directly applied as ANN inputs, once they are also dependent on θ_x. Therefore, only the amplitude (a_x) component can be directly applied as an ANN input, because a_x is independent from θ_x, in this way having no relationship with ω_C. To compensate for memory effects, in [12] the instantaneous (n) and previous (up to the memory length M) samples of the input amplitude are applied as ANN inputs, e.g., $a_x(n-m)$, with m from 0 to M. However, applying only amplitude components as ANN inputs severely deteriorates the modeling accuracy [12]. In other words, the ANN inputs must somehow sense the present and past samples of θ_x in order to provide accurate predictions of phase-modulation-to-amplitude-modulation (PM-AM) and phase-modulation-to-phase-modulation (PM-PM) conversions. The strategy introduced in [12] was to purposely modify the polar angle components prior to their application as ANN inputs, in a way that their relationship with ω_C is completely eliminated. For that purpose, the difference between polar angle components at two consecutive time instants was first calculated, then the sine and cosine were evaluated, and finally, the resulting values, at instantaneous and past samples were applied as independent ANN inputs, e.g., $\sin[\theta_x(n-m_1) - \theta_x(n-m_1-1)]$ and $\cos[\theta_x(n-m_1) - \theta_x(n-m_1-1)]$, with m_1 from 0 to $(M+1)$.

By using the ANN inputs introduced in [12], independent of the ANN architecture (TLP or RBF), only real-valued base-band ($0\omega_C t$) signals are available at the ANN outputs. Therefore, additional computations must be performed to estimate the complex-valued in-band ($1\omega_C t$) envelope signal at the PA output. Indeed, the real-valued ANN estimations have to be first condensed into a single complex-valued base-band signal. Then, a complex-valued base-band signal (centered at zero frequency) must be shifted in frequency to the in-band (centered at ω_C). According to [12], the frequency shifting operation can be done by

$$\tilde{y} = \tilde{s} \exp\left(j\theta_x\right), \tag{12}$$

where $\tilde{s}$ is a complex-valued base-band signal centered at zero frequency, θ_x the polar angle component of the complex-valued input envelope, and $\tilde{y}$ the complex-valued in-band output envelope. Concerning the conversion from real-valued into complex-valued signals, in [12] a polar decomposition was adopted. In particular, the two real-valued outputs (a_s and θ_s) of a single ANN are assumed as the amplitude and polar angle components of the base-band complex-valued signal $\tilde{s}$, according to:

$$\tilde{s} = a_s \exp\left(j\theta_s\right). \tag{13}$$

In [13], a polar decomposition was also used to perform the mapping from real-valued into complex-valued signals, but now the real-valued amplitude (a_s) and polar angle (θ_s) components of $\tilde{s}$ are estimated
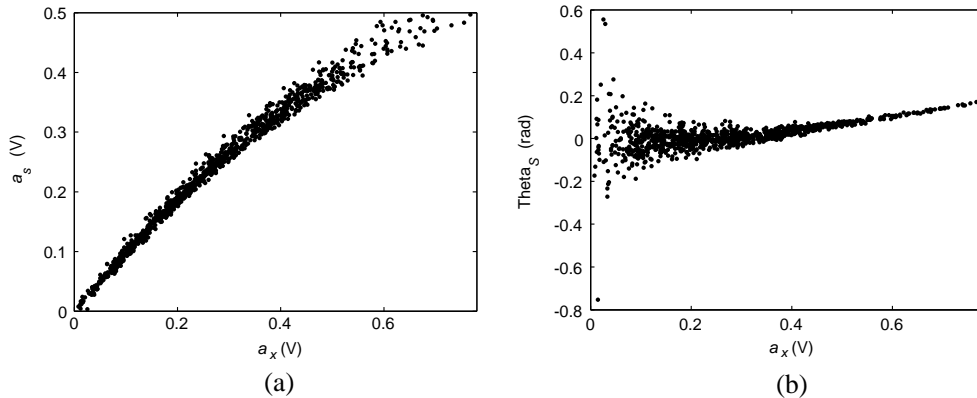
Figure 2. Nonlinear transfer characteristics measured on a GaN HEMT class AB PA excited by a WCDMA signal: (a) amplitude of $\tilde{s}$ as a function of the instantaneous input amplitude, (b) polar angle of $\tilde{s}$ as a function of the instantaneous input amplitude.

by two independent ANNs. In fact, it was observed in [13] that the use of ANNs having single output provides a better trade-off between modeling error and number of network parameters. Nevertheless, in [12, 13], the impact of the conversion from real-valued into complex-valued signals on the accuracy and computational complexity of a low-pass equivalent model was not addressed. In fact, the choice for polar decomposition in the conversion from real-valued to complex-valued signals has no connection with the fulfillment of the band-pass constraint.

Now, it is investigated whether the conversion from two real-valued signals into one complex-valued, performed over the ANN outputs, has any effect on the accuracy and computational complexity of a model. The polar decomposition applied in [12, 13] is first investigated. To that purpose, based on data measured on a GaN HEMT class AB PA excited by a WCDMA signal, Figures 2(a) and 2(b) show the amplitude (a_s) and polar angle (θ_s) components of the base-band complex-valued signal $\tilde{s}$, respectively, as a function of the amplitude (a_x) of the input envelope.

The nonlinear transfer characteristics shown in Figure 2 are, indeed, the nonlinear mappings that each ANN of [13] is intended to mimic. Observe that a single value of the instantaneous input amplitude produces different outputs at distinct time instants. The scattering pattern indicates that the nonlinear mappings are not static, in this way clearly illustrating the presence of memory effects. As a consequence, the instantaneous output depends either on previous samples of the input amplitude (dynamic AM-AM and AM-PM conversions) or on previous samples of the input polar angle (PM-AM and PM-PM conversions). From Figure 2(a), notice that for each value of the input amplitude, the vertical displacement (due to the scattering) is essentially constant at all input amplitude levels. However, from Figure 2(b), a remarkable widening of the vertical displacement is observed at very low input amplitude levels. More important, while θ_s achieves values not larger than 0.2 radians at high input amplitude levels, extremely large values for θ_s (around 0.6 radians) are observed at input amplitude levels near zero. The huge spreading in θ_s values at very low input amplitudes can have a catastrophic impact on the identification of the ANN weights and biases. The reasoning is as follows. In the training of an ANN, the network parameters are chosen in order to minimize the mean square error (MSE) between desired and estimated outputs, according to

$$MSE = \frac{1}{N} \sum_{n=1}^{N} \left| out_s^{des}(n) - out_s^{est}(n) \right|^2, \tag{14}$$

where N is the total number of samples, out_s^{des} the desired output, and out_s^{est} the output estimated by the ANN. The nonlinear training algorithm for the ANN that estimates the polar angle θ_s can be trapped into local minima, specially those local minima that provide excellent estimations for θ_s at very low input amplitudes at the cost of deteriorating the estimations at large input amplitudes. For instance, in the MSE computation a 1% error in a sample at very low input amplitude having θ_s equal to 0.6 radians is equivalent to a 5% error in a sample at high input amplitude having θ_s equal to 0.12 radians.

Notwithstanding, the amount of θ_s deviations at low input amplitude levels is further accentuated by measurement noise.

In summary, the choice for polar decomposition in the conversion from two real-valued signals into one complex-valued signal done in [12, 13] can give rise to non optimal ANN training.

Now, attention is turned to the application of the Cartesian (or rectangular) decomposition to implement the transformation from two real-valued signals into one complex-valued signal. For that purpose, the base-band complex-valued signal $\tilde{s}$ is now constructed from two real-valued signals according to

$$\tilde{s} = \Re_s + j\Im_s, \tag{15}$$

where $\Re_s$ and $\Im_s$ represent the real and imaginary parts of the complex-valued signal $\tilde{s}$, respectively. Using the same data measured on a GaN HEMT class AB PA excited by a WCDMA signal, Figures 3(a) and 3(b) show the real ($\Re_s$) and imaginary ($\Im_s$) components of the base-band complex-valued signal $\tilde{s}$, respectively, as a function of the amplitude (a_x) of the input envelope. Observe that the vertical displacement (due to the scattering) is approximately uniform at all input levels for the two nonlinear transfer characteristics shown in Figure 3. In other words, the huge spreading in θ_s values at very low input amplitudes, clearly observable in Figure 2(b), has no visible consequences on the transfer characteristics shown in Figure 3. Even though $\Re_s$ and $\Im_s$ are dependent on θ_s, at very low amplitude levels their values are primarily determined by the amplitude information a_s. Indeed, $\Re_s = a_s \cos(\theta_s)$ and $\Im_s = a_s \sin(\theta_s)$, and the multiplication of a number close to zero by any number is still a number close to zero. Such information is highly valuable and will be exploited in the sequence for the development of a novel ANN-based low-pass equivalent model. It is worth mentioning that, although Figures 2 and 3 were obtained from a class AB PA, similar behaviors are also expected for PAs operating in different classes (A, B, C, etc.).

The ANN-based low-pass equivalent model proposed in this work is addressed. Figure 4(a) shows a block diagram of the two independent real-valued feed-forward neural network model previously introduced in [13]. A block diagram of the model proposed in this work is shown in Figure 4(b). Observe that Figure 4(b) differs from Figure 4(a) only by the real-valued signals that must be estimated by the ANNs. In particular, in the proposed model a Cartesian decomposition is used to perform the conversion from two real-valued signals into one complex-valued signal. Hence, according to Figure 4(b), one ANN estimates the instantaneous sample of the real part ($\Re_s$) of the base-band complex-valued signal $\tilde{s}$, while another ANN estimates the instantaneous sample of the imaginary part ($\Im_s$) of $\tilde{s}$. Based on the discussion presented in this section, it is expected that the proposed model, in comparison with the previous approach of [13] in a scenario of same number of network parameters, can provide a superior modeling accuracy. Specifically, in the proposed model there is one ANN to map the nonlinear transfer characteristic shown in Figure 3(a) and one ANN to map the nonlinear transfer characteristic shown in Figure 3(b). Therefore, the training algorithms for both ANNs of Figure 4(b) are less susceptible to be trapped into local minima than the training algorithm for the ANN that estimates θ_s in Figure 4(a). Finally, it is worth mentioning that the fulfillment of the band-pass constraint is guaranteed in both
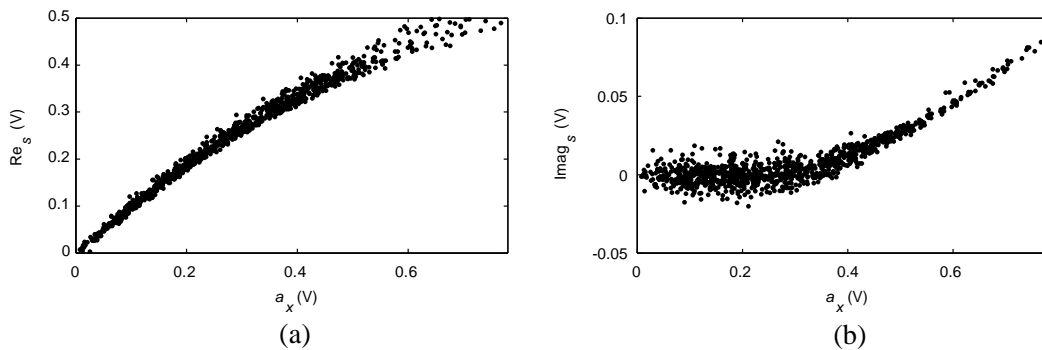
Figure 3. Nonlinear transfer characteristics measured on a GaN HEMT class AB PA excited by a WCDMA signal: (a) real part of $\tilde{s}$ as a function of the instantaneous input amplitude, (b) imaginary part of $\tilde{s}$ as a function of the instantaneous input amplitude.
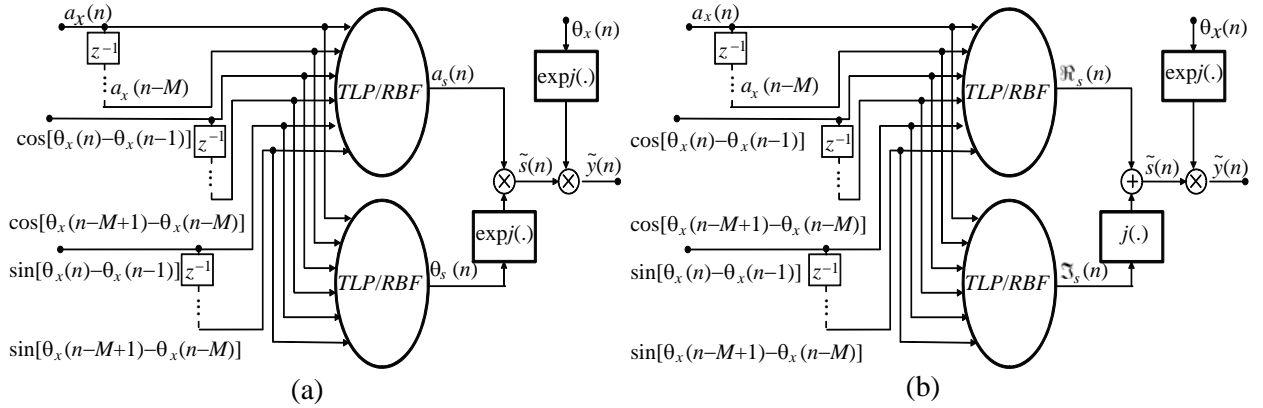
Figure 4. Block diagram of ANN-based PA behavioral models: (a) previous [13] and (b) proposed.

Table 1. NMSE results in dB as a function of the number of network parameters.

Number of parameters	38	47	56	65	74	83	92	101	110	119
previous [13]	-39.9	-40.6	-41.0	-41.6	-42.1	-42.5	-42.7	-43.0	-43.2	-43.3
proposed	-40.8	-41.6	-42.2	-43.0	-43.8	-44.4	-44.8	-45.2	-45.3	-45.5

low-pass equivalent models shown in Figure 4. Indeed, it is the selection of ANN real-valued inputs done in Figure 4 that avoids the generation of out-of-band contributions.

5. EXPERIMENTAL VALIDATION

In this section, the accuracies of the proposed ANN-based model of Figure 4(b) and the previous ANN-based model of Figure 4(a) are compared. To that purpose, a Rohde & Schwarz FSQ vector signal analyzer (VSA) was used to measure discrete-time input-output data sampled at 61.44 MHz from a GaN HEMT class AB PA, excited by a double-carrier WCDMA signal having a bandwidth of 8.84 MHz and centered at 900 MHz, for a PA average output power of 26 dBm.

One part of the measured input-output data was used to train, by the back-propagation algorithm [16], the two ANN-based low-pass equivalent behavioral models shown in Figure 4, having the TLP architecture of Figure 1(a) with the hyperbolic tangent sigmoid activation function given by (7). The memory length was fixed in $M = 2$, but the number of neurons in the hidden layer of the ANNs was varied in order to change the number of network parameters.

The remaining measured input-output data was used to evaluate the normalized mean-square error (NMSE), as defined in [18], between measured and estimated complex-valued output envelopes. Figure 5 and Table 1 show the NMSE as a function of the number of network parameters. Observe that, in case of same number of network parameters, the proposed model of Figure 4(b) is more accurate than the previous approach of Figure 4(a). Indeed, the largest difference between the proposed and previous approaches, quantified by a NMSE difference of 2.2 dB, is achieved if both ANN-based models have 101 real-valued network parameters. Figure 5 and Table 1 confirm that the training algorithms for the proposed model are less susceptible to be trapped into local minima.

Additional confirmations of the quality of the output signal estimated by the proposed model are provided by the power spectral densities (PSDs) shown in Figure 6, the amplitude-to-amplitude (AM-AM) conversions shown in Figure 7 and the amplitude-to-phase (AM-PM) conversions shown in Figure 8. Specifically, in Figures 6, 7 and 8 measured data are compared to data estimated by the proposed model of Figure 4(b) having 110 network parameters. Hence, Figures 6, 7 and 8 clearly show, in different ways, the extremely high accuracy of the proposed model having 110 network parameters.
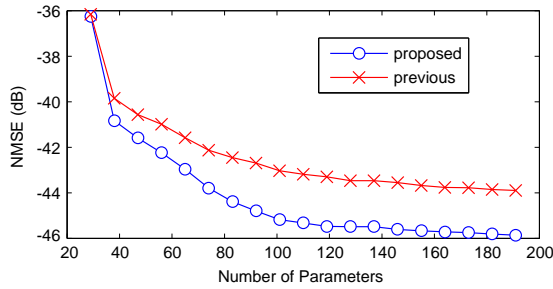
Figure 5. NMSE results as a function of the number of network parameters. The GaN HEMT class AB PA is modeled by TLPs having $M = 2$ and a variable number of neurons in the hidden layer.
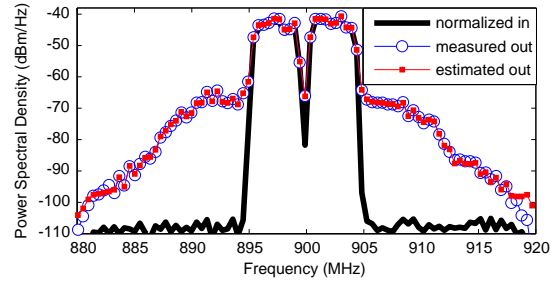
Figure 6. Power spectral densities of the measured and estimated PA output signals. The GaN HEMT class AB PA is modeled by the proposed TLP having $M = 2$ and 110 network parameters.
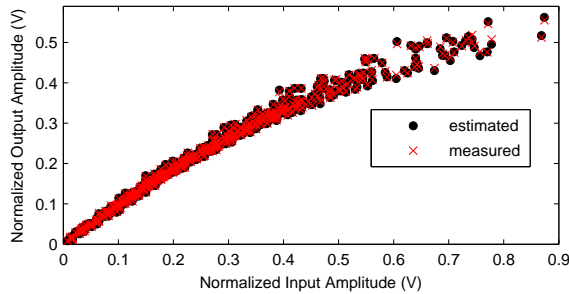
Figure 7. Measured and estimated normalized AM-AM conversions. The GaN HEMT class AB PA is modeled by the proposed TLP having $M = 2$ and 110 network parameters.
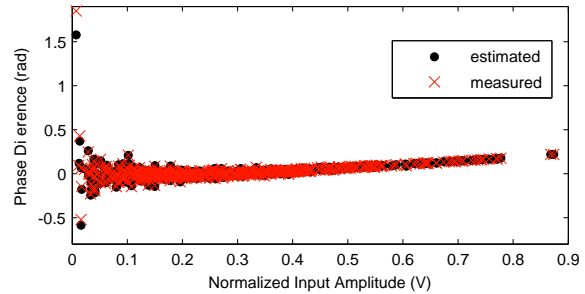
Figure 8. Measured and estimated AM-PM conversions. The GaN HEMT class AB PA is modeled by the proposed TLP having $M = 2$ and 110 network parameters.

6. CONCLUSIONS

This work proposes an ANN-based low-pass equivalent PA behavioral model that can be seen as a modified version of a previous ANN-based approach. In one hand, the ANN real-valued inputs are the same in both previous and modified models in order to guarantee that only in-band contributions (centered at ω_C) are generated by the low-pass equivalent PA behavioral model. On the other hand, the ANN real-valued outputs in the modified model are different from the ANN outputs in the previous approach in order to attenuate the problem of local minima in the ANN training algorithm. The higher accuracy provided by the modified model than the previous approach of same computational complexity is confirmed by a very significant reduction in modeling error, quantified by improvements in NMSE up to $2.2\,\mathrm{dB}$ when applied to fit data measured on a GaN HEMT class AB PA.

ACKNOWLEDGMENT

REFERENCES

1. Raychaudhuri, D. and N. B. Mandayam, "Frontiers of wireless and mobile communications," *Proc. IEEE*, Vol. 100, No. 4, 824–840, 2012.

2. Raab, H., P. Asbeck, S. Cripps, P. B. Kenington, Z. B. Popovic, N. Pothecary, J. F. Sevic, and N. O. Sokal, "Power amplifiers and transmitters for RF and microwave," *IEEE Trans. Microw. Theory Tech.*, Vol. 50, No. 3, 814–826, 2002.

3. Cripps, S., *RF Power Amplifiers for Wireless Communications*, Artech House, Norwood, 2006.

4. Piazzon, L., R. Giofre, P. Colantonio, and F. Giannini, "A method for designing broadband Doherty power amplifiers," *Progress In Electromagnetics Research*, Vol. 145, 319–331, 2014.

5. Kim, J. and Y. Park, "Design of a compact and broadband inverse class-F^{-1} power amplifier," *Progress In Electromagnetics Research C*, Vol. 46, 75–81, 2014.

6. Kenington, P. B., *High Linearity RF Amplifier Design*, Artech House, Norwood, 2000.

7. Pedro, J. C. and S. A. Maas, "A comparative overview of microwave and wireless power-amplifier behavioral modeling approaches," *IEEE Trans. Microw. Theory Tech.*, Vol. 53, No. 4, 1150–1163, 2005.

8. Wang, H., H. Ma, and J. Chen, "A multi-status behavioral model for the elimination of electrothermal memory effect in DPD system," *Progress In Electromagnetics Research C*, Vol. 47, 103–109, 2014.

9. Sun, G., C. Yu, Y. Liu, S. Li, and J. Li, "An accurate complexity-reduced simplified Volterra series for RF power amplifiers," *Progress In Electromagnetics Research C*, Vol. 47, 157–166, 2014.

10. Liu, T., S. Boumaiza, and F. M. Ghannouchi, "Dynamic behavioral modeling of 3G power amplifiers using real-valued time-delay neural networks," *IEEE Trans. Microw. Theory Tech.*, Vol. 52, No. 3, 1025–1033, 2004.

11. Isaksson, M., D. Wisell, and D. Ronnow, "Wide-band dynamic modeling of power amplifiers using radial-basis function neural networks," *IEEE Trans. Microw. Theory Tech.*, Vol. 53, No. 11, 3422–3428, 2005.

12. Lima, E. G., T. R. Cunha, and J. C. Pedro, "A physically meaningful neural network behavioral model for wireless transmitters exhibiting PM-AM/PM-PM distortions," *IEEE Trans. Microw. Theory Tech.*, Vol. 59, No. 12, 3512–3521, 2011.

13. Chipansky Freire, L. B., C. de Franca, and E. G. de Lima, "Low-pass equivalent behavioral modeling of RF power amplifiers using two independent real-valued feed-forward neural networks," *Progress In Electromagnetics Research C*, Vol. 52, 125–133, 2014.

14. Jeruchim, M. C., P. Balaban, and K. S. Shanmugan, *Simulation of Communication Systems — Modeling, Methodology, and Techniques*, Kluwer Academic/Plenum Publishers, New York, 2000.

15. Benedetto, S., E. Biglieri, and R. Daffara, "Modeling and performance evaluation of nonlinear satellite links — A Volterra series approach," *IEEE Trans. Aerosp. Electron. Syst.*, Vol. 15, No. 4, 494–507, 1979.

16. Haykin, S., *Neural Networks: A Comprehensive Foundation*, Prentice Hall, New Jersey, 1999.

17. Chen, S., C. F. N. Cowan, and P. M. Grant, "Orthogonal least squares learning algorithm for radial basis function networks," *IEEE Trans. Neural Netw.*, Vol. 2, No. 2, 302–309, 1991.

18. Isaksson, M., D. Wisell, and D. Ronnow, "A comparative analysis of behavioral models for RF power amplifiers," *IEEE Trans. Microw. Theory Tech.*, Vol. 54, No. 1, 348–359, 2006.